*J. Fluid Mech.* (1982), *vol.* 118, *pp.* 241–268
*Printed in Great Britain*



# The structure of the large eddies in fully developed turbulent shear flows. Part 1. The plane jet

By J. C. MUMFORD

Fluid Dynamics Section, Cavendish Laboratory,
Madingley Road, Cambridge, U.K.

(Received 12 December 1980 and in revised form 7 September 1981)

A series of measurements, obtained using arrays of hot-wire anemometers, has been performed in the fully developed region of a plane turbulent jet. The anemometer output signals were simultaneously sampled, digitized with sufficient resolution for numerical linearization, and recorded on magnetic tape for subsequent analysis.

The data was processed to extract information about the structure of the large eddies within the flow. Firstly, a selection of the two-point velocity correlation functions was evaluated, and diagrams of the contours of constant correlation for the streamwise velocity component were constructed. Secondly, an iterative procedure similar to the techniques generally described as 'pattern recognition and image enhancement' was used to form 'ensemble' averages of the two-dimensional patterns of the streamwise velocity component associated with the large eddies.

The results indicate that the large eddies in the fully turbulent region of the flow are roller-like structures with axes aligned approximately either with the direction of the strain associated with the mean-velocity gradient or with the direction of homogeneity (spanwise). It was found that these basic structures tended to occur in various preferred combinations. Estimates were obtained for the total intensity contribution from the large eddies, the ranges of sizes and intensities of the individual structures, and their effective packing density.

## 1. Introduction

For a wide variety of unsteady flows the presence of organized structures or 'large' eddies within velocity fields exhibiting various degrees of chaos has become a central feature of the formulation of mechanistic or phenomenological models. In cases where the velocities associated with the structures constitute a large proportion of the total intensity of the fluctuations, their existence and degree of organization can usually be demonstrated by flow-visualization techniques. The most familiar example is probably the vortex shedding from a circular cylinder, and in this case observations at various Reynolds numbers and downstream distances reveal ranges of both scales of coherence and relative intensities of the vortices to the remaining motion.

Probably the most objective method of decomposing an arbitrary velocity field into a set of organized structures is that proposed by Lumley (1965), in which the eddies are identified with the eigenfunctions of the correlation matrix. This method, however, suffers from a number of difficulties, and most authors have used an eddy model of the general form described by Townsend (1970, 1976). Although this approach seems to have greater intuitive appeal, the problem of giving an exact specification

of the decomposition of the velocity field is quite complicated. While the word 'organized' has been used in the present description, the structures are more commonly referred to in the literature as 'coherent', and this property is usually defined such that it may be ascribed to an individual structure, without reference to the remainder of the flow field. Partly for this reason, many authors have given the impression that an individual structure may be identified on the basis of some intrinsic property of its own velocity field. This approach is not very helpful since, on the basis of a single example, it is not possible to distinguish between an organized structure and a statistical fluke. Only the relatively frequent recurrence of similar spacially localized velocity patterns indicates organization of the individuals.

In order to express this property more precisely, it is convenient to consider the joint probability density of the velocities simultaneously measured at a large number of points, distributed throughout a volume with linear dimensions somewhat greater than the typical length scales of the flow. The presence of organized structures would imply that, in certain regions of the velocity space, the density is significantly greater than that which would have been obtained by ascribing equal probabilities to all the mechanically possible velocity fields satisfying the same integral constraints as the actual flow. In the case of the vortex shedding from a cylinder, for example, the system is almost always found in the vicinity of a certain closed orbit in velocity space. In considering flows of greater complexity, however, it is clear that, as the number of 'degrees of freedom' of the individual structures increases, the possibility of extracting information about them, or even establishing their existence, becomes more remote. For this reason most experimental investigations have involved flows where the structures are heavily constrained in terms of their possible positions and orientations.

In recent years a considerable amount of investigation has been directed towards the determination of the shapes and internal velocity distributions of the structures occurring in a variety of flows, and a summary of much of this work has been given by Davies & Yule (1975). While it is difficult to generalize, the experiments tend to have been concentrated into three main groups:

(i) structures in mixing layers and jets during their early development;

(ii) structures in the intermittent regions of fully developed shear flows;

(iii) structures in boundary layers closely related to motions near the wall.

In almost all cases, the structures have some 'sharp' feature associated with them, so that they may be identified and located by a relatively simple local condition being satisfied somewhere in the flow. There are, of course, exceptions to this, and more complex detection schemes have been described by a few authors, notably Wallace, Brodkey & Eckelmann (1977) and Townsend (1979).

The large eddies in the fully turbulent regions of the shear flows are somewhat more illusive, for reasons discussed by Blackwelder (1979). Apart from the absence of any sharp identifying features, the intensity of the structures is not particularly large compared with that of the remaining motion. Furthermore, in addition to their positional (and possibly orientational) degrees of freedom, it seems very probable that significant ranges of both sizes and intensities exist for structures of generally similar type. These factors, combined with the difficulty of devising unambiguous flow-visualization experiments, have undoubtedly led to a degree of scepticism about their existence.

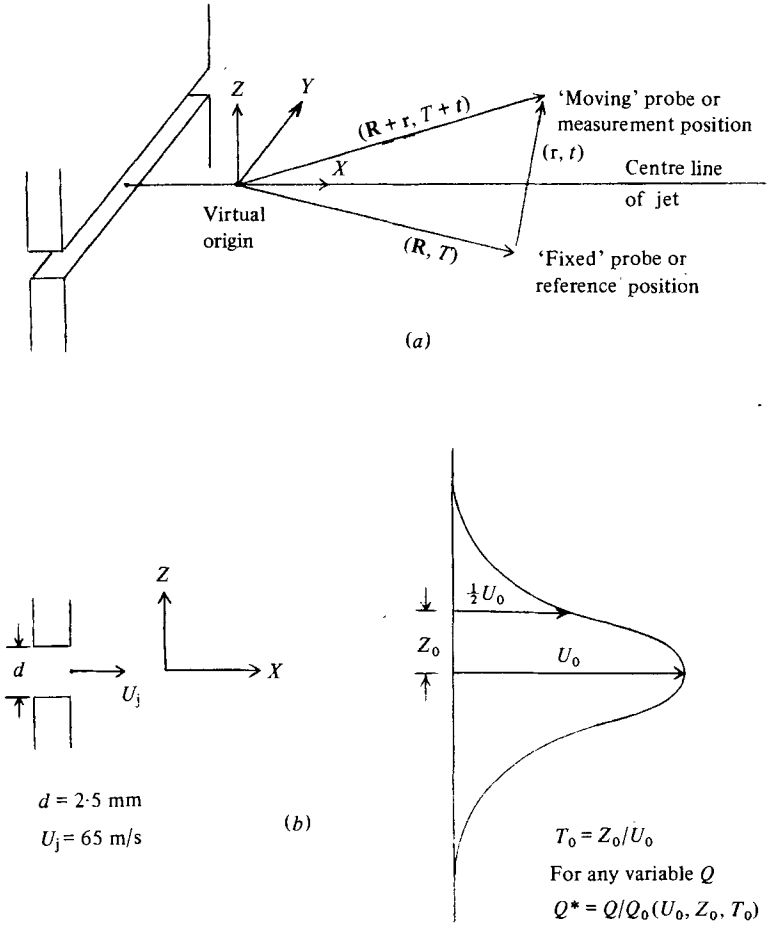


FIGURE 1. Co-ordinate system (*a*) and scaling factors (*b*) for the plane jet.

Attempts to deduce the form of the large eddies in these flows from measurements of the two-point velocity correlation function have been made by Grant (1958) in the plane wake and the boundary layer, and by Mumford (1973) in the plane jet. In addition, Payne & Lumley (1967) have performed the eigenfunction decomposition of Grant's measurements in the wake. In the present series of experiments, data obtained in fully developed shear flows, using an array of hot-wire probes, has been processed to yield 'ensemble' averages of the two-dimensional patterns of the streamwise velocity component associated with the large eddies. The technique, and the results of a number of tests using simulated signals, are described in § 5. The main experimental results for the plane jet are contained in §§ 6 and 7, and the results from other flows are presented in subsequent parts.

## 2. Experimental arrangement: the plane jet

The jet consisted of a slot, 2·5 mm high and 0·4 m wide, in one end of a settling chamber 60 mm high and 0·7 m long. From this the air discharged freely into the room, except for being confined horizontally between two vertical walls 0·4 m apart,

0·55 m high and 0·6 m long. The settling chamber was 0·4 m wide over the final 0·3 m of its length, tapering to 60 mm wide at the inlet. It was fitted with four 1·5 mm mesh wire screens, and was supplied with air from a centrifugal blower via a flexible hose 0·9 m long and 60 mm diameter. The jet speed could be controlled by an adjustable flap over the blower intake, and was normally set at 65 m/s. This gave a Reynolds number based on slot height and exit velocity of approximately $10^4$.

The co-ordinate system used for the experiments, and the scaling factors for the various measurements are illustrated in figure 1. The total velocity will be denoted by $(U, V, W)$, and the fluctuating velocity by

$$(u, v, w) = (U, V, W) - (\overline{U}, \overline{V}, \overline{W}),$$

where an overbar denotes the time average. The measurements were performed at a downstream distance $X$ of 0·4 m (160 slot heights), where the mean velocity $U_0(X)$ on the jet centre plane was 10·7 m/s and the half-width $Z_0(X)$ was 44 mm.

The mean flow uniformity in the $Y$-direction was checked with a total head tube at a number of $(X, Z)$-positions. At $X/d = 160$, the total head variations at $Z = 0$ were within 5 % of the mean over the central 0·3 m of the total width of the flow (0·4 m). At the same position, hot-wire measurements of $(\overline{u^2})^{\frac{1}{2}}$ indicated variations within 5 % of the mean over the central 0·15 m of the flow. The uniformity, however, deteriorated with increasing $Z^*$, and deviations of 10 % were found at $Z^* = 1$.

## 3. Instrumentation

### 3.1. *Hot-wire anemometers*

The velocity measurements were performed with hot-wire probes constructed from Wollaston wire with a core diameter of 2·5 $\mu$m. The wire was etched over a length of approximately 1·5 mm, and this etched section was held under slight tension by the curvature of the surrounding unetched wire. The probes were used with constant-temperature anemometer circuits giving a frequency response 3 dB down at approximately 50 kHz.

The probes were calibrated in a low-turbulence wind tunnel to obtain the variation of anemometer output voltage with flow velocity and, in the case of the X-wires, with flow direction. The velocity dependence was fitted (least-squares) with a curve of the form

$$V^2 = A + BU^{\frac{1}{2}} + CU \tag{3.1}$$

(Bruun 1971), where $V$ is the anemometer output voltage, $U$ is the velocity, and $A$, $B$ and $C$ are fitted constants. The angular dependence was fitted (least-squares) with the function

$$U_{\text{eff}} = U(\cos^2(\theta_0 + \theta) + k^2 \sin^2(\theta_0 + \theta))^{\frac{1}{2}} \tag{3.2}$$

(Champagne, Sleicher & Wehrmann 1967), where $U_{\text{eff}}$ is the 'effective cooling velocity', $U$ is the actual velocity, $\theta$ is the angular deviation (in the plane of the X-wire) from the calibration position, and $\theta_0$ and $k^2$ are fitted constants.

### 3.2. *Signal-processing equipment*

The anemometer outputs (up to 8 channels) were directly coupled via amplifiers with adjustable gain and offset into sample-and-hold circuits. The outputs of these were

| Velocity (m/s) | 5 | 10 | 15 |
|---|---|---|---|
| Resolution ± (m/s) | 0·01 | 0·015 | 0·02 |

TABLE 1

fed via an 8-into-1 analogue multiplexer into a successive approximation digitizer with a resolution selectable at either 8 or 12 bits, with conversion cycle times of 35 $\mu$s and 50 $\mu$s respectively. The frequency response of the combination of amplifiers and sample-and-hold circuits was 3 dB down at 250 kHz.

The digitizer output was recorded on a Precision Instruments Model PI 1400 9-track tape-recorder, fitted with two 4K buffers. This permitted maximum continuous transfer rates of 22 500 samples/s at 8-bit resolution, and 11 250 samples/s at 12-bit resolution.

The tapes were analysed on the University of Cambridge Computing Service IBM 370/165.

### 3.3. *Calculation of the velocities from the digitized voltages*

The velocities were obtained by the exact solution of (3.1) and (3.2). For single straight wires, the $U$-component was calculated from (3.1) as

$$U = \frac{1}{4C^2}[-B+\operatorname{sgn}(C)\{B^2+4C(V^2-A)\}^{\frac{1}{2}}]^2. \tag{3.3}$$

For the range of velocities encountered in the experiments, the typical velocity resolution obtainable using a 12-bit digitizer and a fixed offset voltage is summarized in table 1. For X-wires, the pairs of simultaneously sampled voltages $V_i$ ($i = 1, 2$) were converted into corresponding 'calibration' velocities $U_i$ using (3.3) with constants $A_i$, $B_i$ and $C_i$. These velocities are *not* the actual velocities experienced by the probe, but the velocities that would have been required in the calibration tunnel (with the probe at its calibration angle) to produce the observed voltages. Using $S$ to denote the resolved component of the total velocity in the plane of the X-wire, (3.2) gives

$$U_1(\cos^2\theta_{01}+k_1^2\sin^2\theta_{01})^{\frac{1}{2}} = S(\cos^2(\theta_{01}+\theta)+k_1^2\sin^2(\theta_{01}+\theta))^{\frac{1}{2}},$$
$$U_2(\cos^2\theta_{02}+k_2^2\sin^2\theta_{02})^{\frac{1}{2}} = S(\cos^2(\theta_{02}-\theta)+k_2^2\sin^2(\theta_{02}-\theta))^{\frac{1}{2}},$$

where $\theta$ is the deviation of the direction of $S$ from the calibration angle.

These simultaneous equations for $S$ and $\theta$ were solved for each pair of voltage samples, and the velocity components obtained from

$$U = S\cos\theta \quad \text{and} \quad V \text{ or } W = S\sin\theta.$$

## 4. Correlation measurements

The correlation function for two arbitrary flow variables $p$ and $q$ is defined by

$$R_{pq}(\mathbf{R},\mathbf{r},t) = \frac{\overline{p(\mathbf{R},T)\,q(\mathbf{R}+\mathbf{r},T+t)}}{(\overline{p(\mathbf{R},T)^2}\,\overline{q(\mathbf{R}+\mathbf{r},T)^2})^{\frac{1}{2}}},$$

where the overbar denotes the time average. For the plane jet, the value of $Y$ is irrelevant, and the property of self-preservation (Townsend 1976) implies that changing

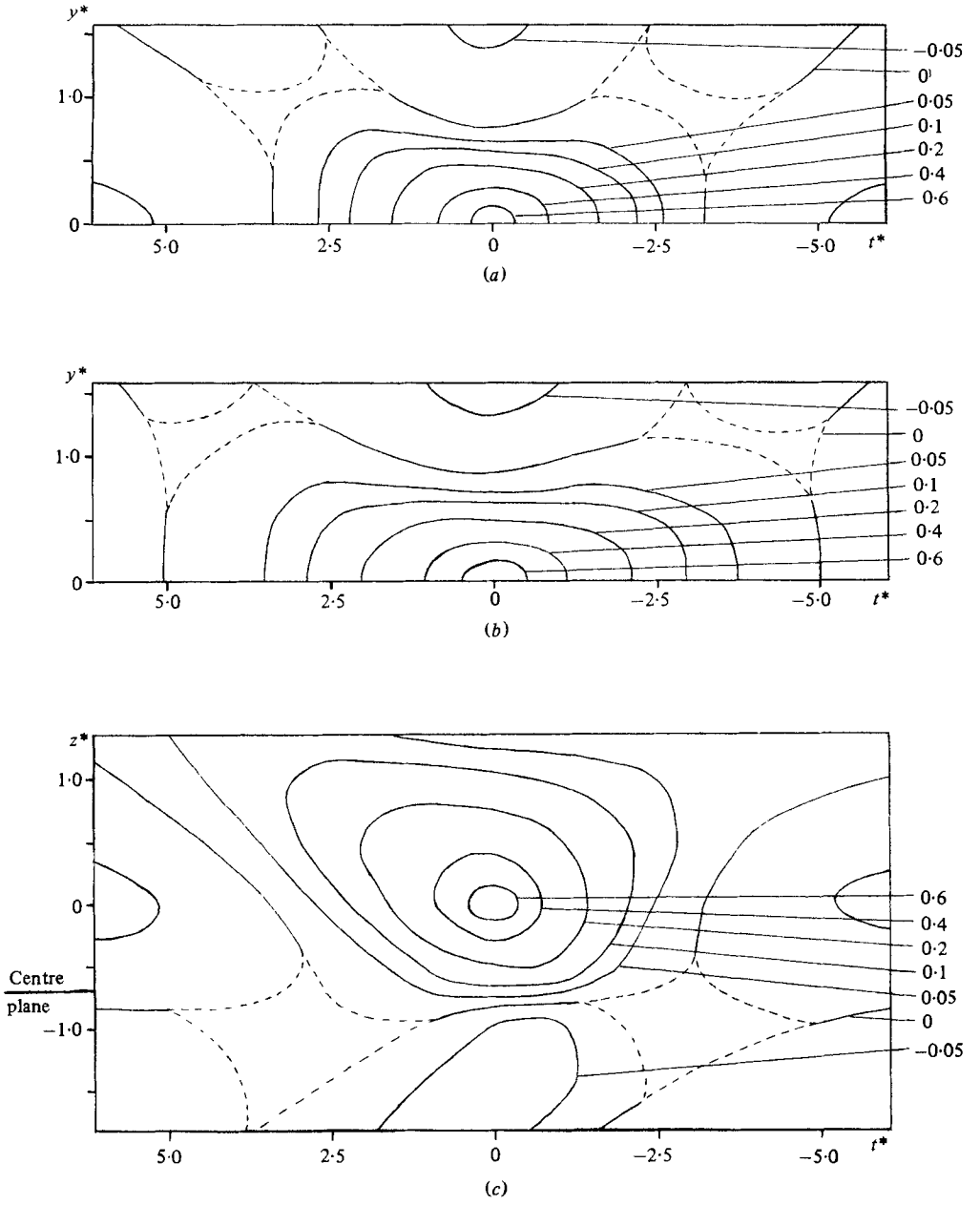


FIGURE 2. Contours of constant $R_{uu}(0{\cdot}67, (0, y^*, 0), t^*)$ (*a*), $R_{uu}(1{\cdot}0, (0, y^*, 0), t^*)$ (*b*) and $R_{uu}(0{\cdot}67, (0, 0, z^*), t^*)$ (*c*).

$X$ simply changes the scales of $Z$, $\mathbf{r}$ and $t$. (This property was demonstrated experimentally in Mumford 1973.) The correlation function will therefore be written as $R_{pq}(Z^*, \mathbf{r}^*, t^*)$. Using the eight probes in a row parallel to either the $Y$- or $Z$-directions, the $R_{uu}$ correlation was evaluated over the $(y, t)$- and $(z, t)$-planes respectively. Some of the results are shown as contours of constant correlation in figures 2(*a*) ($R_{uu}(0{\cdot}67, (0, y^*, 0), t^*)$), 2(*b*) ($R_{uu}(1{\cdot}0, (0, y^*, 0), t^*)$), 2(*c*) ($R_{uu}(0{\cdot}67, (0, 0, z^*), t^*)$). The regions in the diagrams enclosed within the dashed contour lines represent saddle points where

the correlation is close to zero. A much longer averaging time would have been required to determine which of the two possible interconnections of the zero contours is correct.

The results are in good agreement with those presented in Mumford (1973), which were obtained at $X/d = 40$ using an $x$-displacement instead of a time delay. The general features of the correlation maps are also very similar to those obtained by Kovasznay, Kibens & Blackwelder (1970)† for the turbulent boundary layer on a flat plate. It should be noted, however, that other boundary-layer measurements (Grant 1958; Tritton 1967)† suggest that $R_{uu}(Z,(x,0,0),0)$ is always positive in the fully turbulent region of the flow, so that the negative values of $R_{uu}(Z,\mathbf{0},t)$ found by Kovasznay *et al.* for large $|t|$ may not have a simple interpretation in terms of the eddy structure.

In order to explain the shapes of the correlation maps in the jet, it was suggested in Mumford (1973) that the large eddies consisted of roller-like structures having a component of circulation in the $(x,y)$-plane and axes in the $(x,z)$-plane at angles of approximately $\mathrm{sgn}\,(Z) \times 135°$ to the $X$-axis (figure 11*a*). By using a combination of such single rollers and contrarotating pairs with their axes displaced in the $X$-direction (figure 11*b*) it was possible to account for the $R_{uu}$ correlations in the $(x,y)$-plane and half the $(x,z)$-plane. While the flow patterns in figure 11 have been depicted parallel to the $(x,y)$-plane, from the $R_{uu}$ measurements alone, no inference can be made regarding the distribution of the $w$ velocity component. Consequently, the flow patterns may well be inclined to the $(x,y)$-plane (figure 5), so that their vorticity is more nearly parallel to the roller axes, and may also have curvature in the $(x,z)$-plane. An arrangement of this sort appears to be generally consistent with the shapes of the contours of constant $R_{ww}(Z,(x,y,0),t)$ and $R_{uw}(Z,(x,y,0),t)$‡ found by Kovasznay *et al.* (1970) in the fully turbulent region of the boundary layer. In addition, these 'strainwise' rollers have a number of features in common with the large eddies found by Grant (1958) in the plane wake.

The negative correlation obtained between points on opposite sides of the jet centre plane is, however, in marked contrast with the behaviour found in the wake, where the roller eddies continued across the centre plane, making $R_{uu}(Z^*,(0,0,z^*),0)$ positive over the entire width of the turbulent region. In the jet, provided $Z^*$ was not too small, $R_{uu}(Z^*,(0,0,z^*),0)$ changed sign when $z^* \simeq -Z^*$, indicating that the contributing structures have only a small range of possible positions in the $Z$-direction. The shapes of the 0·0 and $-0{\cdot}05$ contours in figure 2(*c*) give some indication that the region of negative correlation is aligned with the roller axes. From the $R_{uu}$ correlations alone, however, it is not clear whether this feature is associated with the strainwise rollers or with some additional structures of a different type. The most obvious possibility is the presence of 'spanwise' rollers, having a circulation in the $(x,z)$-plane, centred approximately at $Z = 0$. A sequence of such structures, alternating in sign, would appear as a flapping motion, which has been suggested as a possible constituent of the jet by a number of investigators.

In an attempt to find evidence for motions of this type, measurements of correlations involving the transverse velocity components were performed. Some of the results are shown in figure 3(*a*)

$$(R_{wu}(0,(0,0,z^*),t^*) \quad \text{for} \quad z^* = 0{\cdot}67 \text{ and } 1{\cdot}1)$$

and 3(*b*)
$$(R_{ww}(Z^*,(0,0,1{\cdot}1),t^*) \quad \text{for} \quad Z^* = 0 \text{ and } -0{\cdot}55).$$

† For comparison with the present work, most authors have the $Y$- and $Z$-axes interchanged.

‡ $R_{vv'}(X_0,0,Z,T)$ and $R_{ur'}(X_0,0,Z,T)$ in the reference.

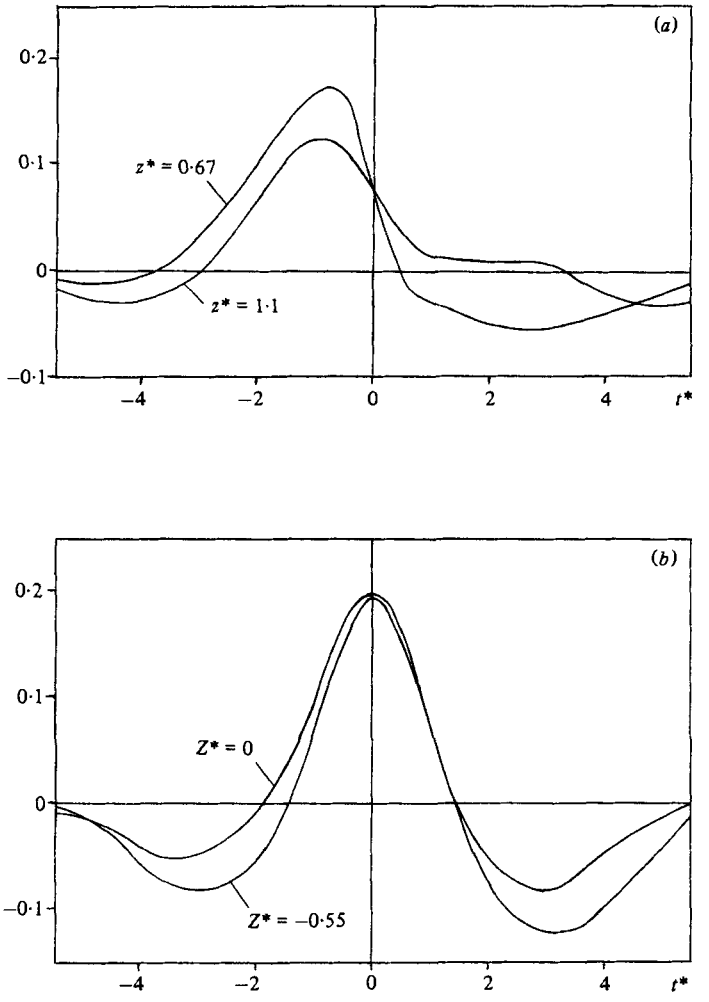


FIGURE 3. The correlations $R_{wu}(0, (0, 0, 0{\cdot}67), t^*)$, $R_{wu}(0, (0, 0, 1{\cdot}1), t^*)$ (*a*) and $R_{ww}(0, (0, 0, 1{\cdot}1), t^*)$, $R_{ww}(-0{\cdot}55, (0, 0, 1{\cdot}1), t^*)$ (*b*).

The presence of spanwise rollers should yield characteristic shapes (figure 4) for these correlations. An example of this is given by Sabot and Comte-Bellot (1976), who found $R_{wu}$ ($R_{12}$ in their notation) curves of this type in turbulent pipe flow. Casual examination of figure 3 indicates that, while $R_{ww}$ has the expected form, $R_{wu}$ is consistent only with the upstream half of the spanwise roller pattern. There are, however, two detailed features of the $R_{wu}$ curves that suggest an alternative explanation:

(i) the positions of the negative regions at negative $t^*$ are consistent with a contribution from the paired strainwise rollers;

(ii) at certain values of $t^*$ the curvature is quite large, which suggests contributions from two (or more) types of structure, differing in scale (Townsend 1976).

While the precise distribution of the $w$ velocity component within the strainwise rollers is unknown, the general features of the $R_{wu}(0, (0, 0, z^*), t^*)$ correlation contributed by these structures will be of the form illustrated in figure 5, and the principal

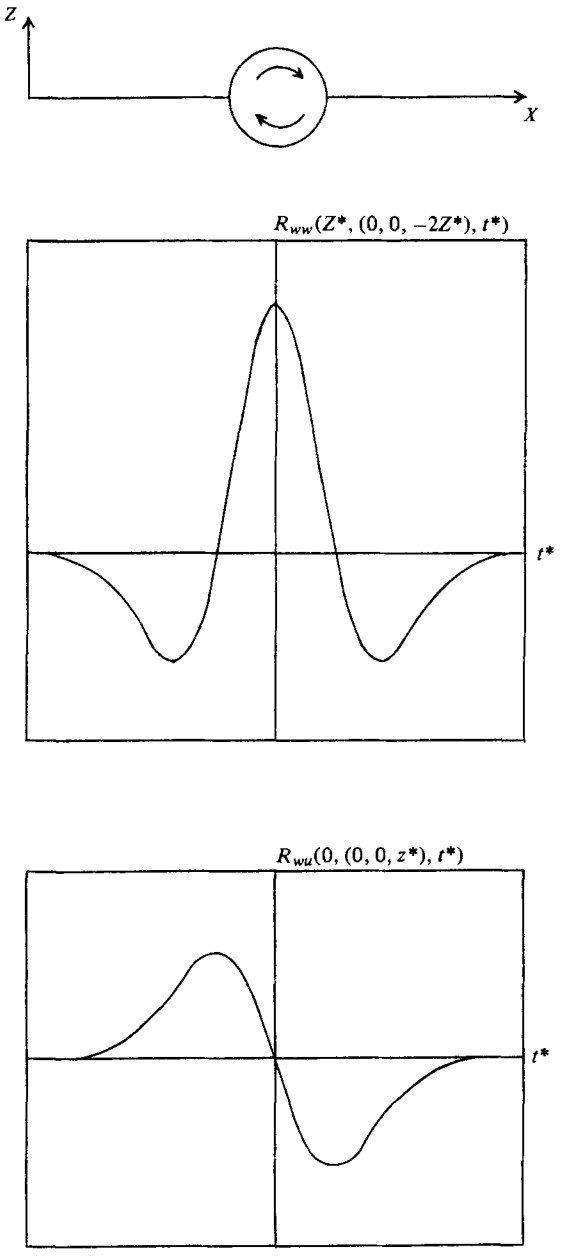


FIGURE 4. The $R_{ww}$ and $R_{wu}$ correlations for spanwise rollers.

effect of increasing $z^*$ will be to shift the entire curve towards more positive values of $t^*$. For the spanwise rollers in figure 4 the effect of increasing $z^*$ will be to change the amplitude of the $R_{wu}$ curve, and increase its spread along the $t^*$ axis (Sabot & Comte-Bellot 1976). The features of the curves in figure 3(*a*) are thus consistent with the presence of both strainwise and spanwise rollers; the relatively small values of $R_{wu}$ obtained for positive $t^*$ being due to a degree of cancellation between the two contributions.

A similar effect may have occurred for some of the $R_{uu}(Z^*, (0, y^*, 0), t^*)$ correlations.

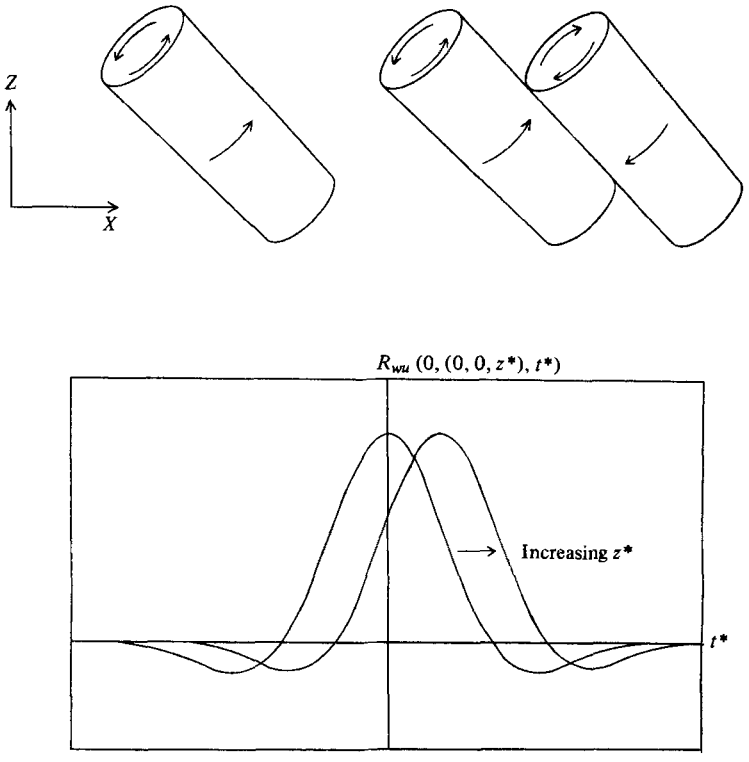


FIGURE 5. The $R_{wu}$ correlation for a combination of single and paired strainwise rollers.

Provided the spanwise structures are coherent over a sufficient distance in the $Y$-direction, they will make a positive contribution to $R_{uu}(Z^*, (0, y^*, 0), 0)$ at values of $y^*$ where this correlation is negative. A tentative estimate of the coherence length of these structures can be obtained from the variation of $R_{uu}(Z^*, (0, y^*, -2Z^*), 0)$ with $y^*$, and a value of approximately $3Z_0$ was found. (This figure seems consistent with the estimate of the packing density of the strainwise rollers given in § 7.)

The orientations and positions of the two types of structure naturally suggest the possibility that they are joined together, and evidence for this is presented in § 6. The velocity patterns in the $(x, z)$-plane produced by this arrangement are shown in figure 13. The correlation map (figure 2*c*) obtained with the reference probe at $Z^* = 0{\cdot}67$ will contain contributions from the patterns $1A$, $1B$, $C$ and $2B$ (in figure 13), the $2B$ contribution giving the alignment of the region of negative correlation for $Z < 0$ with the strainwise rollers. The correlation maps obtained with the reference probe at somewhat larger values of $Z^*$ contained corresponding negative regions for $Z < 0$, but these were of smaller amplitude and showed no obvious alignment, indicating that the principal contributions were from patterns $1A$ and $1B$.

The interpretation of the correlation measurements becomes increasingly uncertain for values of $Z^*$ exceeding approximately 1·5. This is partly because of the contribution from the large-scale motions associated with the entrainment of irrotational fluid, and partly because of the intermittency of the turbulence. For the correlations, the most significant effect is caused by the difference between the 'zone-averaged'†

† For a definition see Kovasznay *et al.* (1970).

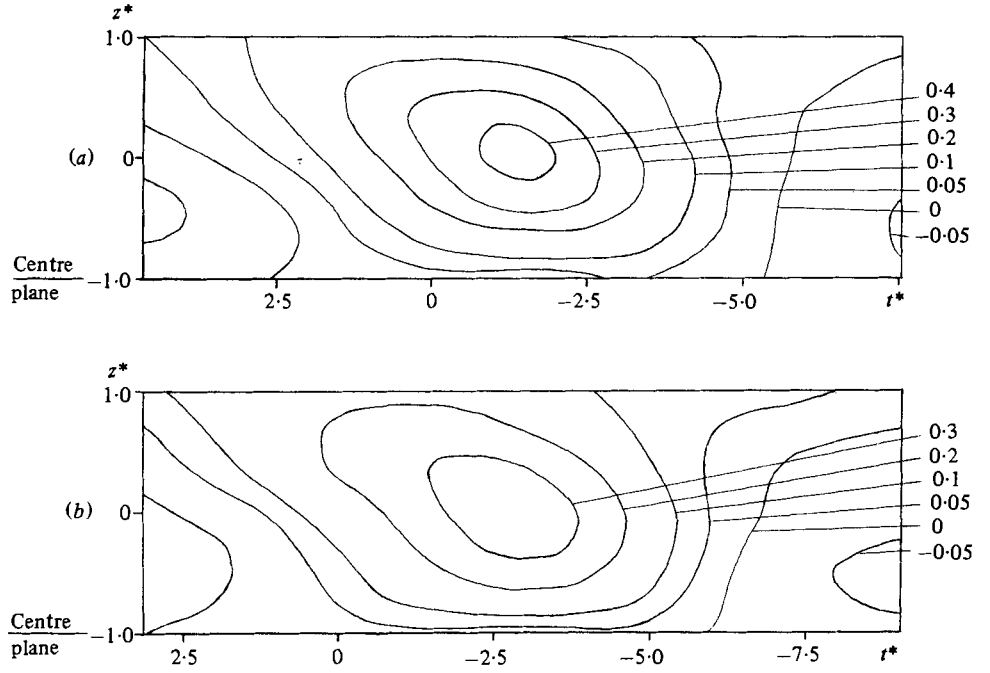


FIGURE 6. Contours of constant $R_{uu}(1{\cdot}0, (1{\cdot}0, 0{\cdot}2, z^*), t^*)$ (*a*) and $R_{uu}(1{\cdot}0, (2{\cdot}0, 0{\cdot}2, z^*), t^*)$ (*b*).

mean velocities in the turbulent and irrotational parts of the flow. From measurements of the zone-averaged probability densities of $u$, it was shown in Mumford (1973) that this difference is sufficiently large to account for almost $0{\cdot}5\overline{u^2}$ at $Z^* = 2{\cdot}0$. Under these circumstances, the forms of the correlations involving the $u$-component may be determined more by the shapes of the turbulence interface than by the flow patterns within the turbulent fluid.

Some information about the development of the large eddies as they are convected downstream can be inferred from space–time correlations, and contour maps of $R_{uu}(1{\cdot}0, (x^*, 0{\cdot}2, z^*), t^*)$ are shown in figures 6 (*a*) ($x^* = 1{\cdot}0$) and 6 (*b*) ($x^* = 2{\cdot}0$). These results were obtained using a rake of seven probes aligned in the $Z$-direction, and displaced from the eighth probe by $x^*$ in the stream direction, and by a distance of approximately $0{\cdot}2Z_0$ in the $Y$-direction to avoid the effects of the wake of the upstream probe. The rapid decay of the maximum (i.e. optimum-delay) correlation with downstream distance is a property common to all the 'high intensity' flows (see e.g. Wygnanski & Fiedler 1969; Fisher & Davies 1964), and a discussion of the expected behaviour of the space–time correlation function has been given by Townsend (1970). While the contribution from the small-scale components is rapidly lost, the contours drawn at heights $\lesssim 0{\cdot}2$ change rather slowly with downstream distance. This suggests that the large-scale structures tend to preserve not only their size and shape but also their orientation in the $(x, z)$-plane, over the range of $x^*$ and $t^*$ covered by the experiments. A similar result was found in the boundary layer by Kovasznay *et al.* (1970), although Sternberg (1967) has given a rather different interpretation of the results obtained by Favre, Gaviglio & Dumas (1957, 1958) in the same flow. Some values of the apparent convection velocity for the structures in the jet are given in Mumford (1973).

## 5. Determination of the structure of the large eddies

### 5.1. *General principles*

While the two-point correlation functions may give a strong indication of the types of large eddies to be found in the various flows, the amount of detail available is necessarily very limited. This is because the contribution to the correlation function $R_{pq}(\mathbf{R}, \mathbf{r}, 0)$ is obtained by multidimensional integration of the eddy velocity cross products over (at least) all possible eddy positions, and is consequently extremely insensitive to the detailed structure of the eddy velocity fields. Any procedure that attempts to deduce the form of these fields from measured correlation functions is therefore subject to considerable uncertainty.

The use of an array of probes, to enable the simultaneous measurement of the fluid velocity at a number of positions, should yield the required structural resolution, provided suitable methods of analysis can be developed. The traditional techniques of turbulence analysis when applied to an array of probes, to yield multipoint correlations, multidimensional probability densities, multiple conditionally sampled averages, etc., seem to suffer from a number of practical difficulties, not least of which is the problem of presenting the results in a form that is readily assimilated.

The method employed in the present investigation attempts to form ensemble averages of the large eddies, to yield two-dimensional maps of the $u$-component of the eddy velocity fields. To achieve this, it is first necessary to identify and locate the large eddies which are randomly positioned in the random velocity field of the remaining turbulent motion. The procedure, consequently, has many features in common with the techniques of 'pattern recognition' and 'image enhancement', which have in recent years been used on a wide selection of scientific problems, though with varying degrees of success.

Using eight probes equally spaced in a row parallel to either the $Y$- or $Z$-directions, the data may be considered as a two-dimensional map of the $u$-component of velocity over the $(x, y)$- or $(x, z)$-planes respectively (see figure 7). The necessity of using a time delay instead of an $x$-displacement suggests that the data will only be a good approximation to the instantaneous velocity field if the 'frozen pattern' approximation (Taylor's hypothesis) is valid. In the jet, this is not the case, as the 'moving-frame autocorrelation' initially falls quite sharply with downstream distance. In the present context, however, we require only that the approximation holds for the large-scale structures under investigation, even though it is not valid for the smaller-scale motions. The results from § 4 indicate that the large eddies change relatively slowly with downstream distance, so that the frozen-pattern approximation should be quite reasonable for these structures.

Starting with an initial guess at the eddy-velocity pattern (based on either visual inspection of the data or correlation measurements), the data is scanned to find occasions on which the velocity field gives a relatively good match to this pattern. This set of velocity fields is taken as the ensemble from which a first estimate of the average is obtained. The initial guess is then replaced by this average, and the process is iterated until it converges.

There is, unfortunately, no guarantee that such a procedure will be practicable for

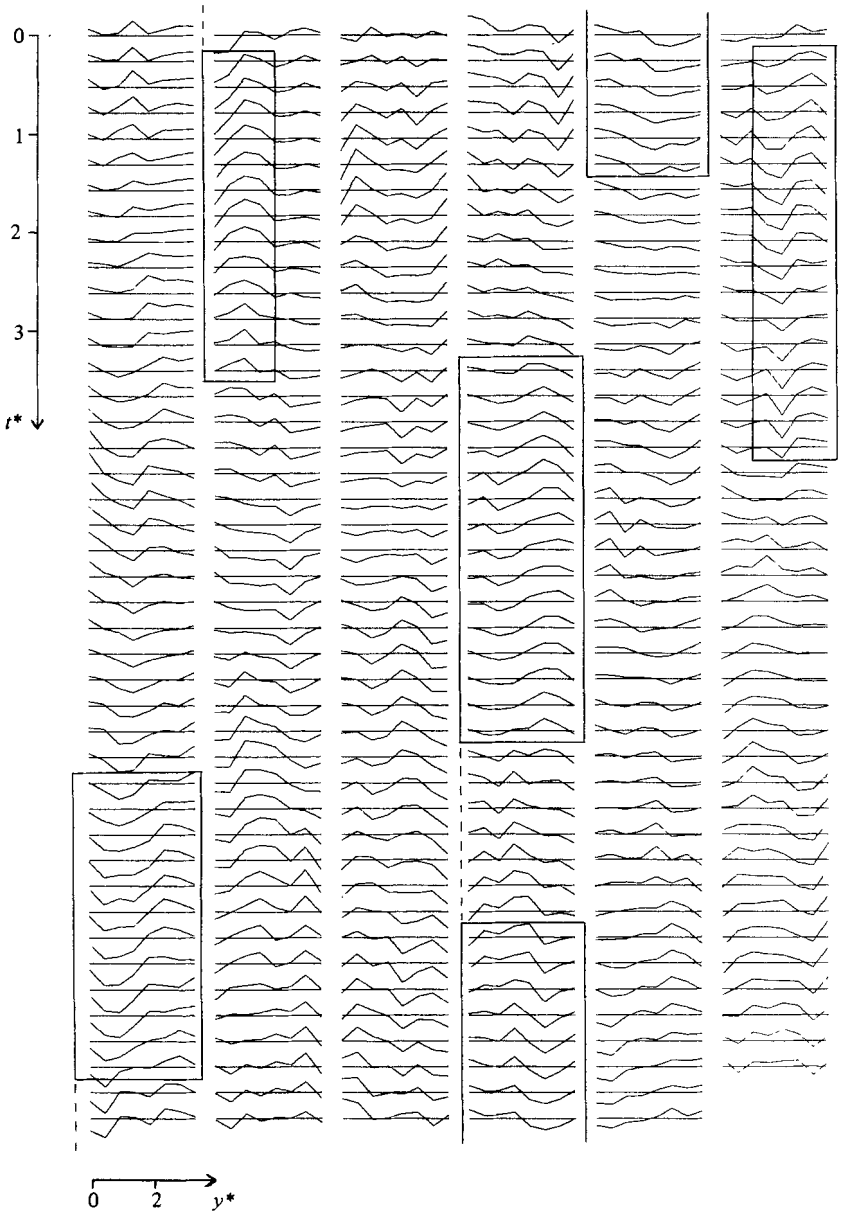


FIGURE 7. Instantaneous velocity 'profiles' in the plane jet. Probe rake in the $y$-direction at $Z^* = 0{\cdot}67$. (Patterns in boxes are of the type contributing to the conditional average in figure 10*b*.)

the fully developed turbulent shear flows, since the statistical properties of the turbulence which determine the success or failure of the method are amongst the properties that the method is hoped to reveal. The results must therefore be shown to satisfy a number of conditions relating to both the experimentally selectable 'inputs' (probe spacing in the flow, threshold levels in the pattern-recognition programme etc.) and the implied statistical properties of the large eddies in the turbulence (distribution of sizes, distribution of intensities, etc.).

In the present investigation, the matching of the 'test' pattern with the data is assessed on the basis of the convolution of the two velocity fields. There are, of course, a number of alternative matching criteria that could have been used, but the convolution method has the simplifying property that the selection of matching patterns does not depend on the amplitude of the test pattern. Whatever method of selection is employed, the presence of a range of sizes, orientations and intensities for structures of a given type will mean that any average is subject to the weighting implied by the method of selection. In particular, the use of the convolution means that for structures of a given size only the most intense examples will be selected, and that the minimum intensity required for selection is size-dependent.

In addition, the presence of a range of sizes in the ensemble will limit the resolution available in the average, even if the various practical limitations, which will become apparent in the following sections, could be overcome.

### 5.2. *Summary of operations in the programme*

From the original data, the mean velocity is calculated for each of the eight channels, and subtracted to yield the fluctuations $u_{ij}$ for $i = 1, \ldots, 8$ and $j = 1, \ldots, 32K$ (typically). These signals are then individually low-pass filtered and scaled with their respective r.m.s. values to give an array denoted by $u'_{ij}$. The filtering was performed by a method which simulates the action of an $n$-stage 'CR' filter giving a roll-off of $6n$ dB/octave. In most cases, a single stage was used with a cut-off frequency (3 dB down) at $0{\cdot}4F_0$ (typical value). This corresponds to a time constant approximately $1\frac{1}{2}$ times the streamwise grid spacing on the velocity contour maps.

The use of a filter is not essential, but gives a reduction in the scatter of the results. The selection of the cut-off frequency has to be something of a compromise. A reduction in the amplitude of the higher-frequency (smaller-scale) components in the data will reduce both the uncertainty in the positions of the patterns and the statistical scatter on taking the ensemble average. Excessive filtering will, however, reduce the available structural resolution.

Using $U_{mn}$ ($m = 1, \ldots, 12$ typically and $n = 1, \ldots, 32$ typically) to denote the 'test' pattern or initial guess, and an asterisk (*) to denote an externally selectable option, the following operations are performed.

(i) Form the set of all convolutions

$$C_{kl} = \sum_{\substack{i=1,\ldots,8 \\ n=1,\ldots,n_{\max}}} u'_{i,n+k-1} U_{i+l-1,n}$$

for

$$l = 1, \ldots, m_{\max} - 7 \quad \text{and} \quad k = 1, \ldots, j_{\max} - n_{\max} + 1.$$

(ii) For this set, calculate the r.m.s. value ($= C_{\mathrm{rms}}$) and the flatness factor.

(iii) For each $k$, find the value of $l$ ($= l_{\max}$) corresponding to either

($a$) the largest $C_{kl}$

or*

($b$) the largest $|C_{kl}|$

(depending on symmetry).

(iv) Find the values of $k$ giving either ($a$) $C_{kl_{\max}}$ or ($b$) $|C_{kl_{\max}}|$ greater than some selected number* of $C_{\mathrm{rms}}$.

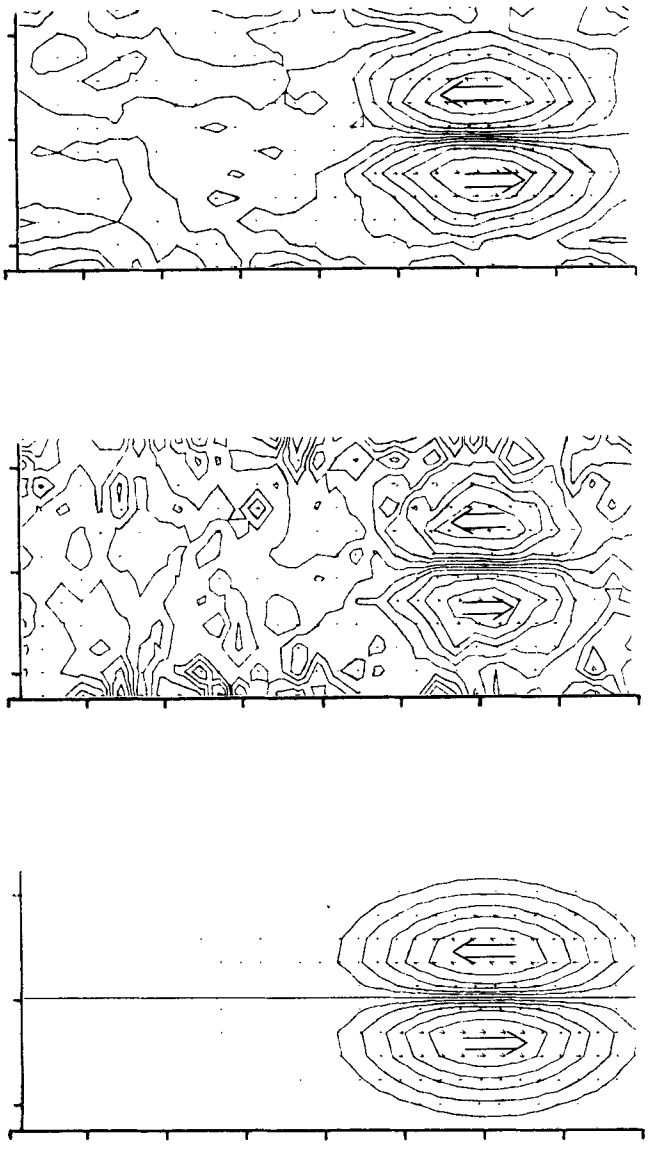


FIGURE 8. Test using normally distributed random numbers.

Defining a 'burst' to be set of one or more successive occasions on which this condition is satisfied, perform the following operations.

(v) Select bursts with lengths in a specified range*.

(vi) For each such burst, find the value of $k$ corresponding to either the centre or* the maximum of either (*a*) $C_{kl_{\max}}$ or (*b*) $|C_{kl_{\max}}|$.

(vii) Form the ensemble average from these values of $k$ by adding (or, for option (*b*) in the case of negative $C_{kl_{\max}}$, subtracting) the corresponding velocity patterns $u'_{ij}$ ($i = 1, \ldots, 8, j = k, \ldots, k+31$) in transverse positions determined by $l_{\max}$, and dividing each column of the resulting pattern by the number of times it has been incremented.

The pattern is then plotted as a scaled diagram with an arrow at each grid point

indicating the magnitude and direction of the $u$-component, and contours of constant $u$ drawn at values $\pm 0{\cdot}7$, $\pm 0{\cdot}5$, $\pm 0{\cdot}35$, $\pm 0{\cdot}25$, $\pm 0{\cdot}1$, and 0 times the peak velocity in the pattern. Unfortunately, many of the arrows are too small to be reproduced reliably, and some large arrows indicating direction but *not* magnitude have been added for clarity, in particular, at positions of local maxima.

### 5.3. *Testing with simulated signals*

The only satisfactory method for checking that the programme functions correctly, and for assessing its performance of the task for which it was designed, is by testing with numerically generated data of known statistical properties. Possibly the most unusual feature of the procedure described in § 5.2 is that there is no absolute criterion for the 'goodness of fit' required for inclusion in the average – a 'relatively' good fit is sufficient. Under these circumstances it is clear that a pattern bearing some sort of resemblance to the original will be extracted from data consisting of totally random numbers, or, equivalently, a pattern would be extracted from turbulence which did not contain organized structures. An essential test, therefore, is to apply the programme to data consisting of normally distributed random numbers. Some of the results of this are shown in figure 8. The central diagram was obtained from totally random numbers, and the upper diagram from random numbers that had been filtered so that their spectral energy distribution was similar to that of turbulence. As expected, the results are simply 'noisy' replicas of the initial guess, with no obvious indications of any systematic change of size or shape in the filtered case. In the unfiltered test, such changes would be impossible to detect.

In order to test the efficiency with which the programme would extract organized structures, a series of simulated signals was used. These consisted of arrays of normally distributed random numbers with superimposed 'eddies' in random positions. The eddies consisted of small arrays of numbers representing a velocity field of the type depicted in the lower diagram of figure 9(*a*). This type of structure ('box eddy') was used in preference to something more realistic because it enables the resolution of fine detail to be assessed. A series of tests was performed to determine the effects of

(i) the amplitude of the eddies relative to the r.m.s. of the random numbers;
(ii) the packing density of the eddies;
(iii) the exclusion of overlaps in the random positioning of the eddies;
(iv) a distribution of eddy sizes;
(v) a distribution of eddy intensities;

and various combinations of these. It was originally hoped that it would be possible to infer some of the statistical properties of the eddies in turbulence by producing simulated signals which, on processing, would yield values for the derived statistics (flatness factors of convolutions etc.) similar to those for the turbulence signals. This technique was not very productive for the fully developed shear flows in the present investigation, but could well be useful for flows containing structures whose typical amplitudes relative to the r.m.s. of the remaining motion are somewhat larger. One result that could be inferred, however, was that, in order to obtain matching statistics as indicated above, it was necessary to impose the constraint that the eddies did not overlap (Townsend 1979).

Some results obtained from one of the simulated signals are shown in figures 9(*a*, *b*).

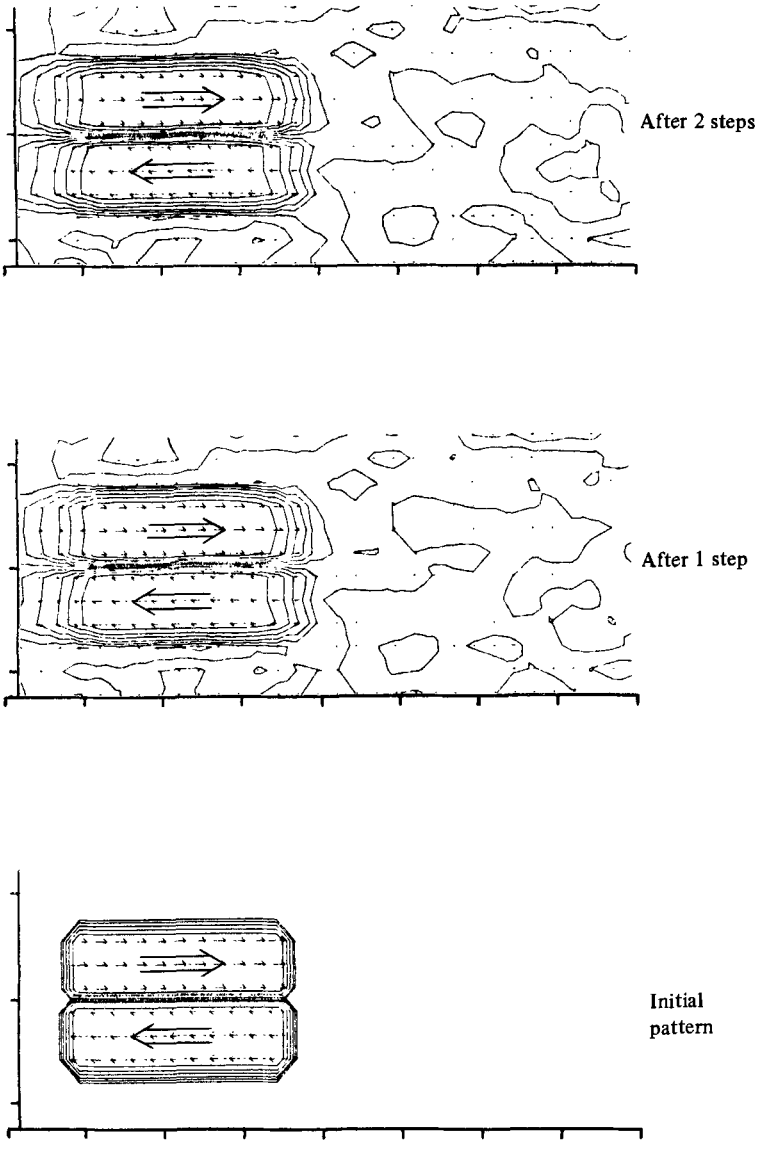


(*a*)

FIGURE 9 (*a*). For caption see p. 258.

In both cases the eddies were all of the type shown in the lower diagram of figure 9 (*a*), and had velocities of + and − the r.m.s. value of the random numbers. They were randomly positioned but subject to the condition that they did not overlap, and covered 5 % of the total area of the random number array. At this packing density and intensity, the eddies give a contribution to $\overline{u^2}$ of approximately 5 %. Figure 9 (*a*) shows the result of applying the programme to this data, using an eddy of the type that was actually present as an initial guess. It should be remembered that some of the loss of resolution in the $x$-direction is due to the filter. A more revealing test is shown in figure 9 (*b*), for which the same data was used, but with a less inspired initial

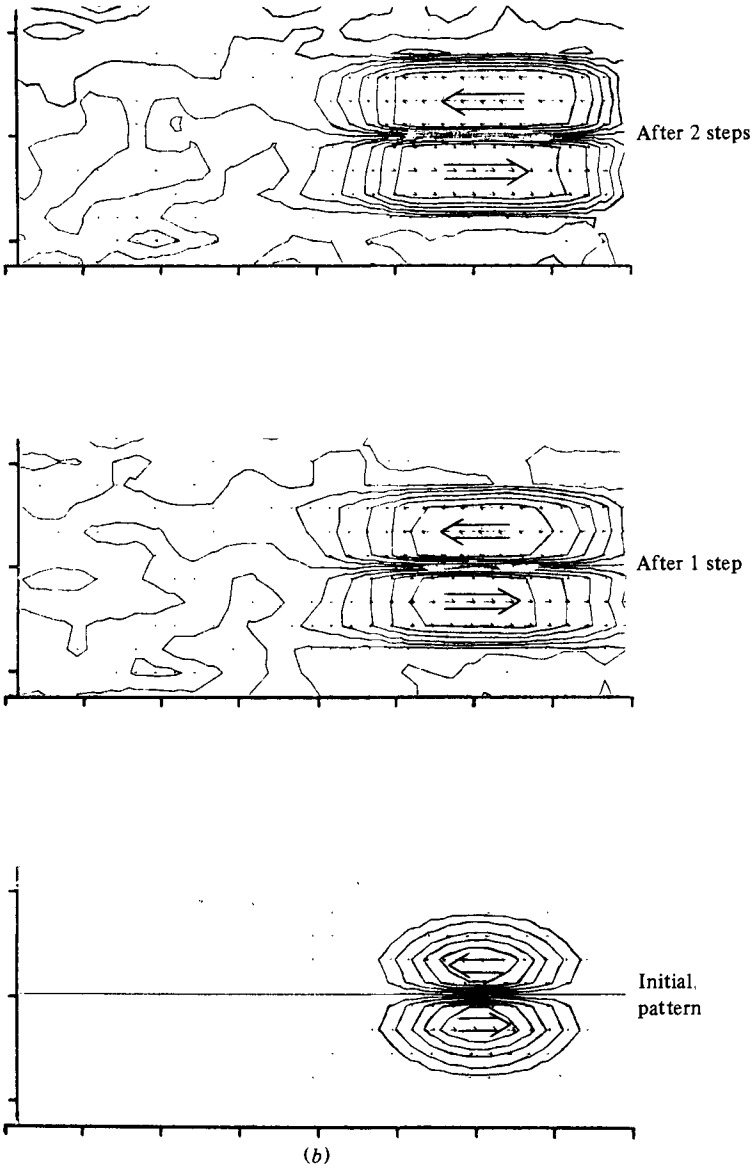


FIGURE 9. Test using normally distributed random numbers with superimposed 'box eddies' in random positions.

guess. It can be seen that, after two applications of the programme, the result is almost identical to that obtained with a perfect initial guess.

## 6. The large eddies in the plane jet

With the probe rake aligned with the $Y$-direction, data was obtained for two probe spacings ($0{\cdot}22Z_0$ and $0{\cdot}44Z_0$) at five values of $Z^*$. Inspection of the velocity traces (figure 7) and the form of the correlation maps (figure 2) suggests flow patterns having

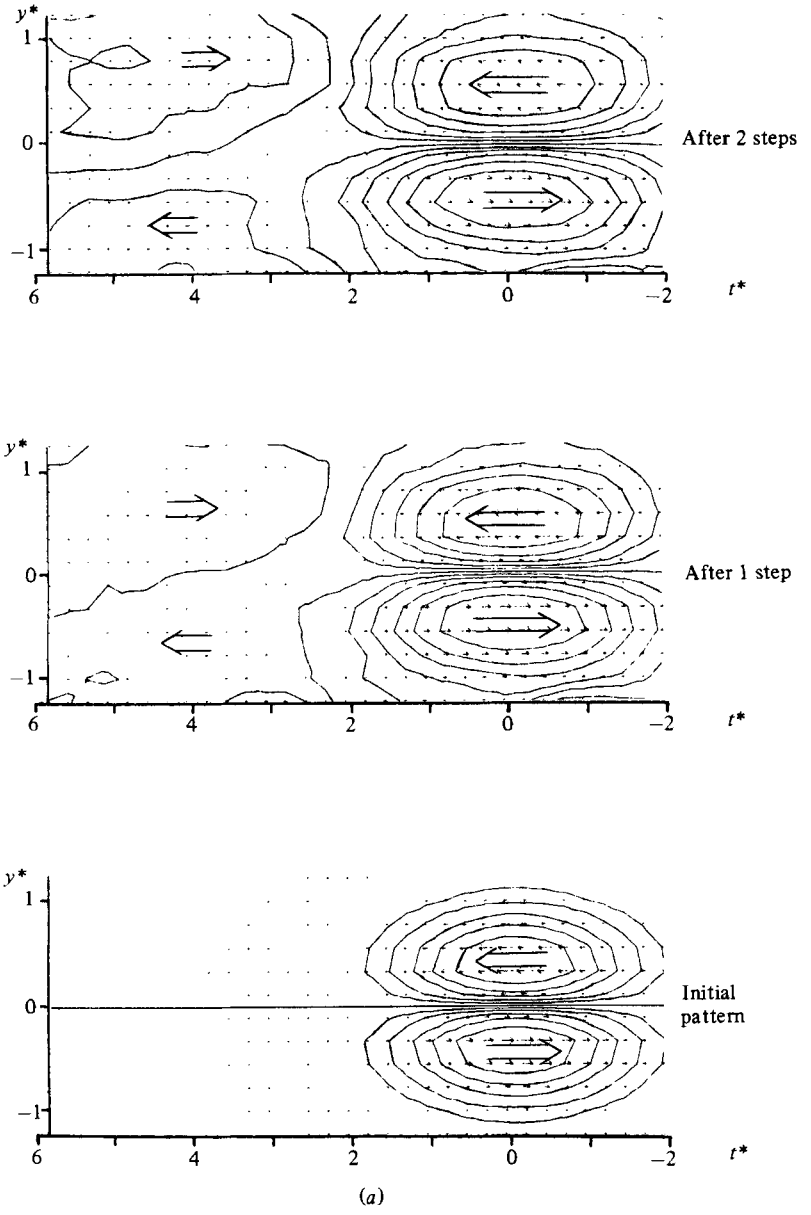


(*a*)

FIGURE 10 (*a*). For caption see p. 261.

a large-scale circulation in the $(x, y)$-plane. Accordingly, the data was processed using test patterns of the form

$$u(x, y) = k_y y \exp\left[-\tfrac{1}{2}(k_x^2 x^2 + k_y^2 y^2)\right],$$

where the constants $k_x$ and $k_y$ determine the longitudinal and transverse scales of the pattern. The processing was performed for a range of values of $k_x$ and $k_y$, and for a range of settings of the adjustable parameters in the programme. The effects of these variations are discussed in § 7.

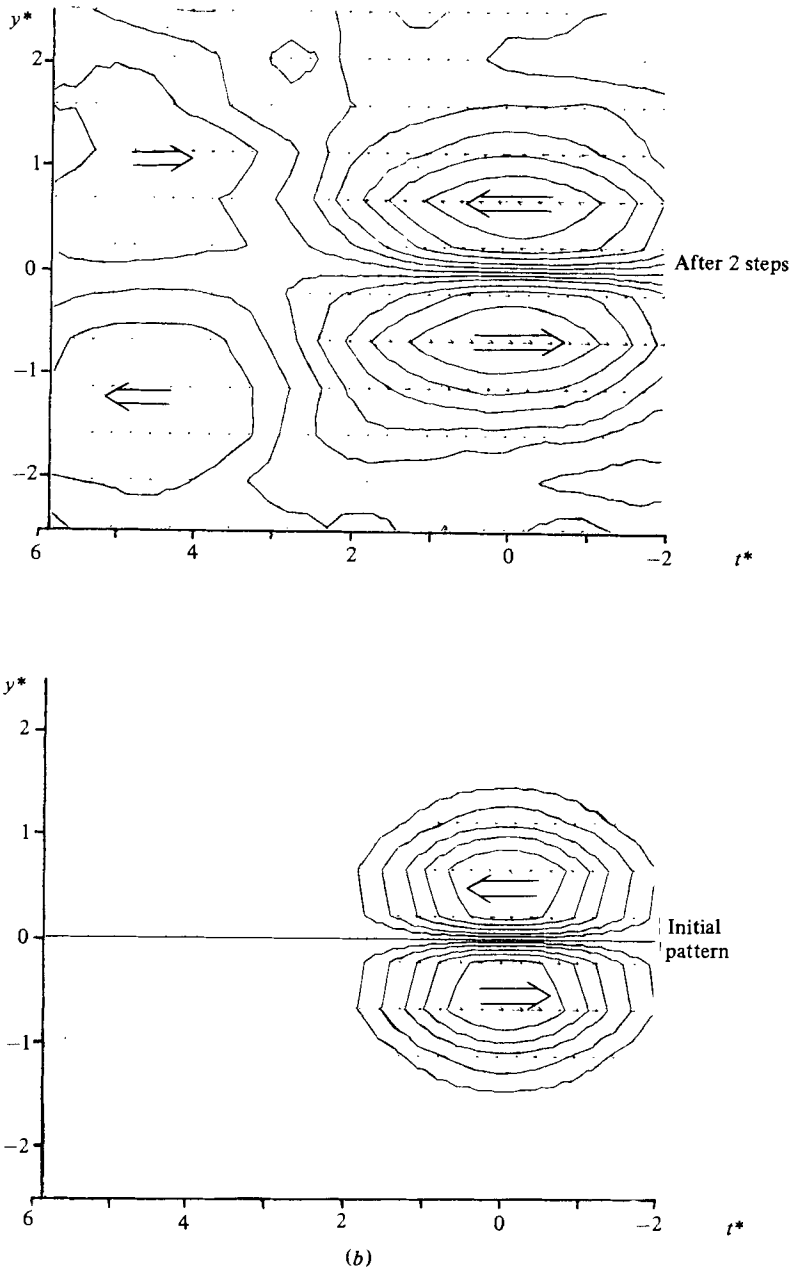


(*b*)

FIGURE 10 (*b*). For caption see p. 261.

Some of the results are shown in figures 10(*a*) ($Z^* = 0{\cdot}33$, narrow probe spacing), 10(*b*) ($Z^* = 0{\cdot}67$, wide probe spacing) and 10(*c*) ($Z^* = 1{\cdot}0$, wide probe spacing). Results from the two different spacings at the same value of $Z^*$ were in good agreement, except possibly where the patterns obtained with the wide spacing show obvious signs of insufficient resolution. While it is clear that the scale of the patterns increases with increasing $Z^*$, the results are otherwise very similar. In each case, in addition to the changes in size and shape from the initial pattern, an extra velocity field is pro-

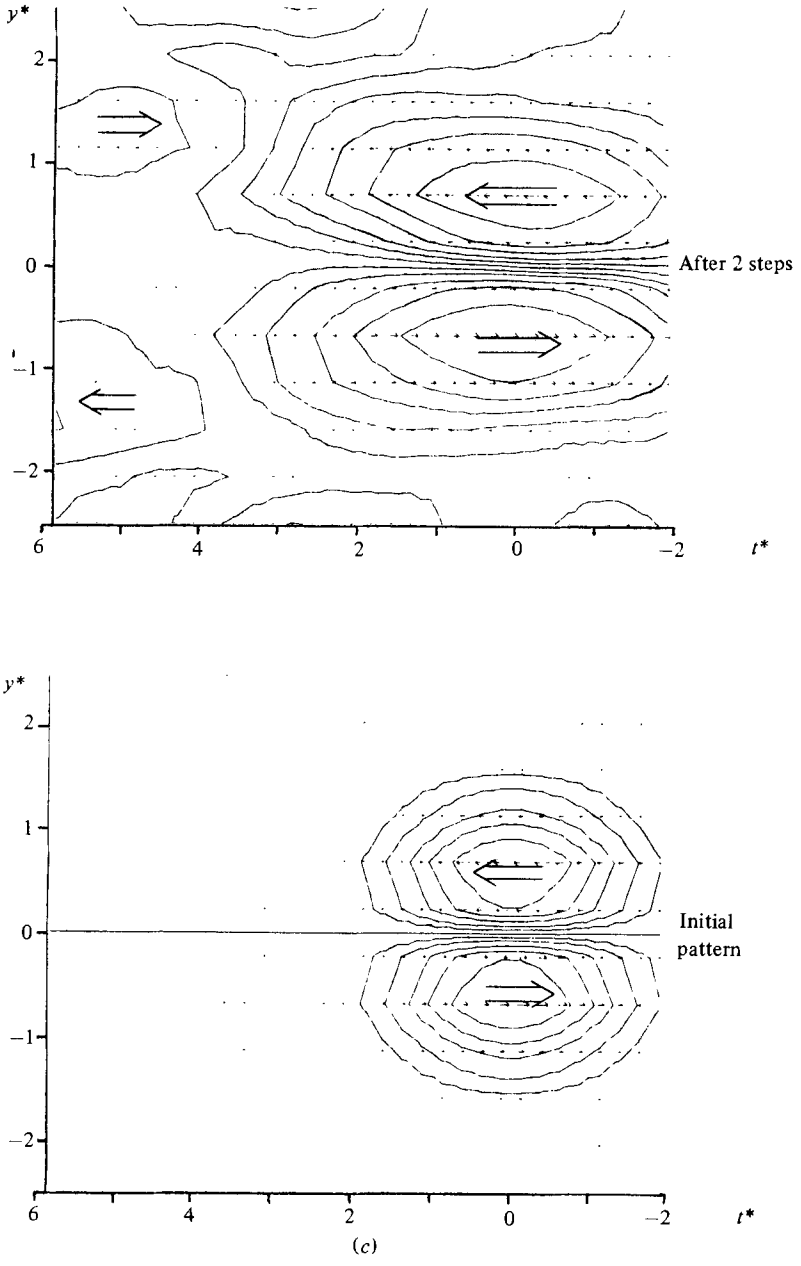


FIGURE 10. Patterns in the $(x, y)$-plane at (*a*) $Z^* = 0{\cdot}33$; (*b*) 0·67; and (*c*) 1·0.

duced. This is displaced in the stream direction from the original pattern, and has velocity peaks in the opposite sense. It appears, therefore, that the result inferred from the correlation measurements was substantially correct, and that the structures responsible for the flow patterns in the $(x, y)$-plane tend to occur in pairs. There are, however, two possible pairing configurations that would yield the observed results:

(i) separation in the $x$-direction, approximate alignment in the $y$-direction, and opposite circulations (figure 11*b*);

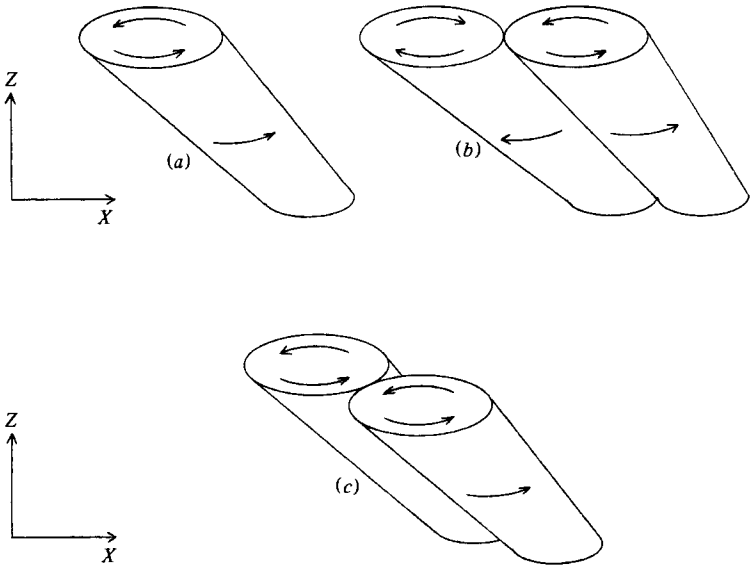


FIGURE 11. The strainwise roller eddies.

(ii) separation in both $x$- and $y$-directions and similar circulations (figure 11$c$).

The latter configuration would be expected to produce two additional velocity peaks either side of the manufactured parts of the patterns. Unfortunately, the transverse ($y$) range covered by the measurements was insufficient† to detect these. Visual inspection of the velocity traces suggests the occurrence of both types.

It should be noted that, following the first application of the programme, the test pattern used for the second step contains the velocity field corresponding to a mixture of single and paired structures. The selection of patterns for the second step will be weighted slightly in favour of the paired type, since, for a given amplitude, these will yield a larger value for the convolution. An estimate of the relative frequency of occurrence of pairs, based on the amplitude of the manufactured part of the pattern obtained after two steps, will therefore tend to be too high.

As in the case of the correlation measurements, the similarity of the patterns obtained at different values of $Z^*$ suggests the presence of roller-type structures, having axes in the $(x, z)$-plane at some as-yet undetermined angle (estimated from the correlations at 135°) to the $X$-axis. Accordingly, the data obtained with the probe rake aligned with the $Z$-direction was processed using test patterns of the form

$$u(x,z) = \begin{cases} \exp\left[-\tfrac{1}{2}k_x^2(x-sz)^2\right] & (Z < 0) \\ 0 & (Z > 0), \end{cases}$$

representing a slice parallel to the $(x, z)$-plane through a roller confined to one side of the jet centre plane, inclined at $180° - \arctan s^{-1}$ to the $X$-axis, and with a longitudinal scale determined by $k_x$. Unlike the test patterns used in the $(x, y)$-plane, where the width was typically 11 probe spacings, allowing 5 possible transverse

† Since an increase in the probe spacing would lead to an unacceptable loss of resolution, a larger number of probes would be required to increase the range.

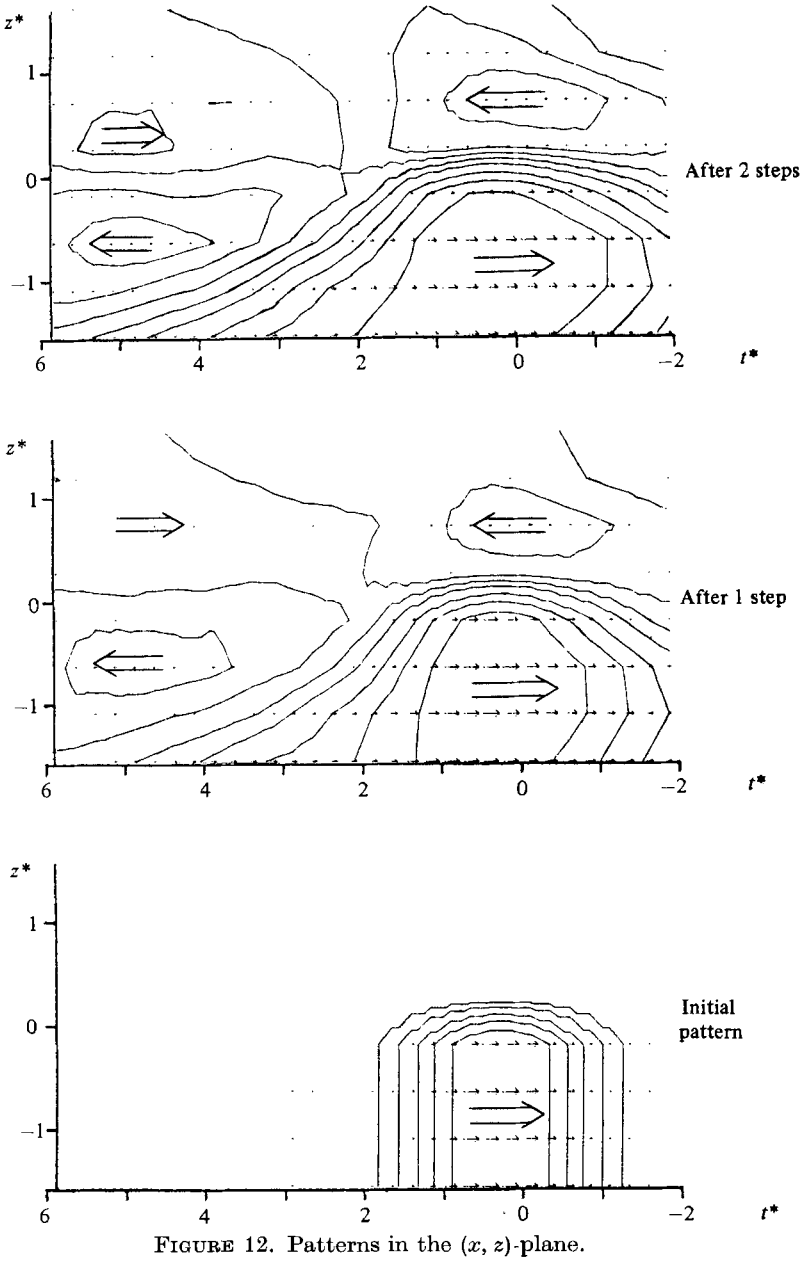


FIGURE 12. Patterns in the $(x, z)$-plane.

positions for the data, the test patterns in the $(x, z)$-plane were 7 probe spacings wide, allowing no transverse alignment. This is because the structures are assumed to be 'locked' in position in the $Z$-direction, while being randomly positioned in the $Y$-direction.

The processing was performed for various values of $k_x$ and $s$, and some of the results for $s = 0$ are shown in figure 12. It should be remembered that the velocity fluctuations $u(\mathbf{R}, T)$ have been scaled with $(\overline{u^2(Z)})^{\frac{1}{2}}$. The results indicate that the roller axes occur at a range of angles to the $X$-axis, centred at approximately 140° and covering perhaps $\pm 15°$. These values are somewhat speculative, firstly because they depend on the

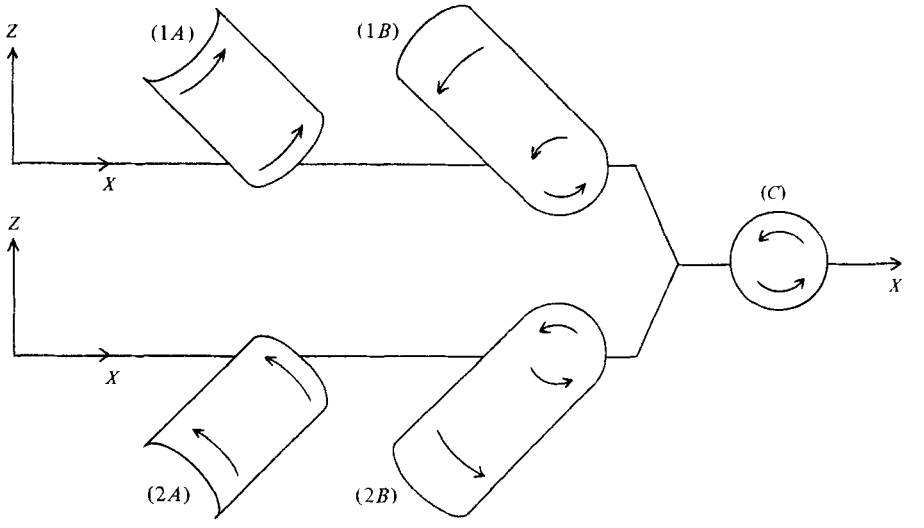


FIGURE 13. Velocity patterns in the $(x, z)$-plane at various $y$-sections ($A$, $B$ and $C$) through strainwise/spanwise combinations (1 and 2).

convection velocities obtained from the space–time correlations, and secondly because the pattern selection procedure is weighted towards structures covering the largest area of the test pattern.

In the region $Z < 0$, the additional velocity field generated outside the original pattern corresponds to the pairing in the $(x, y)$-plane. For $Z > 0$, the generated velocity field is consistent with the correlation contour map of the $(x, z)$-plane (figure 2*c*), and indicates that the velocity fields of the strainwise and spanwise rollers occur simultaneously, implying that the two types are joined together. The various velocity patterns in the $(x, z)$-plane corresponding to different $y$-positions within this arrangement are shown in figure 13 (the paired structures are not shown). For the initial pattern in figure 12 the selection should have been confined to types $2A$ and $2B$, which (in combination with the paired structures) would yield an ensemble average very similar to the experimental result. Just as in the case of the correlation measurements, however, there is some evidence of alignment of the velocity field for $Z > 0$ in figure 12 ($Z < 0$ for the correlations in figure 2*c*) with the strainwise rollers. While it is possible that some of the selected patterns were of type $1B$ (and, by implication, type $C$), the probability of this should have been fairly small (unlike the case of the correlations). An alternative possibility is the occasional occurrence of pairs of strainwise rollers having circulations in the same sense, situated on opposite sides of the jet centre plane, and joined together by a short spanwise section. The velocity pattern near the centre of such an arrangement would appear as a combination of the $1B$ and $2B$ velocity fields (joined at $Z = 0$), which would have a high probability of being selected for inclusion in the average.

The steepness of the velocity gradient $\partial u/\partial z$ in the averaged pattern, across the centre plane, provides justification for the assumption that the structures are 'locked' in position in the $Z$-direction.

It should be noted that while both senses of circulation are equally probable for the strainwise structures, the individual spanwise structures may have a preferred sense

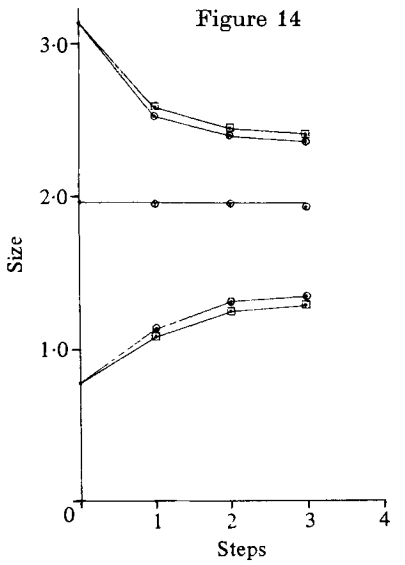


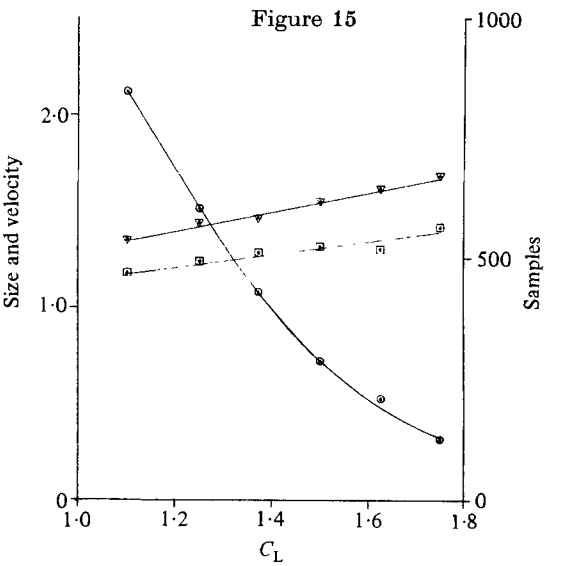


FIGURE 14. Variation of pattern size with number of programme steps for $C_L = 1{\cdot}25$ (⊡) and $1{\cdot}5$ (⊙).

FIGURE 15. Variation of pattern size (⊡), maximum velocity (▽), and numbers of samples (⊙) with inclusion limit.

which depends on whether their centres are located at positive or negative values of $Z$. In addition, while the various possible orientations of the strainwise/spanwise combinations are equally probable, a given orientation may have a preferred sense for the circulation. These possibilities have not been investigated.

## 7. Statistical properties

The convergence property of the programme, and the dependence of the final average on the initial pattern are illustrated in figure 14. The size of the pattern has been (arbitrarily) defined as half the length of the half-velocity contour, and this is plotted in units of $Z_0$ against the number of programme steps for three different starting patterns and two different settings of the inclusion limit $C_L$ in the programme. It seems that the distributions of eddy intensities and sizes are such that convergence is obtained to within a range of sizes, and, as one would expect, this range becomes narrower with increasing $C_L$. The variation with the number of samples (shown implicitly in figure 15) is, however, rather slow, so that there is a relatively well-defined range of sizes in which structures commonly occur with reasonably large amplitude. Structures with sizes outside this range occur less frequently for a given amplitude, or with smaller amplitude for a given frequency.

For the structures shown in figure 11 the definition of size in terms of the length of the pattern in the $X$-direction may be slightly misleading. For rollers of a given 'diameter', the length of the pattern in the $(x, y)$-plane will depend on the angle of the roller axis, and a proportion of the spread of sizes indicated in figure 14 will certainly be due to the range of angles suggested in § 6.

Using a fixed test pattern, the variation of the size and intensity of the ensemble averages (after two steps) with the inclusion limit $C_L$ is shown in figure 15. The sizes represent the lower limit of the range of convergence, and the intensities are expressed

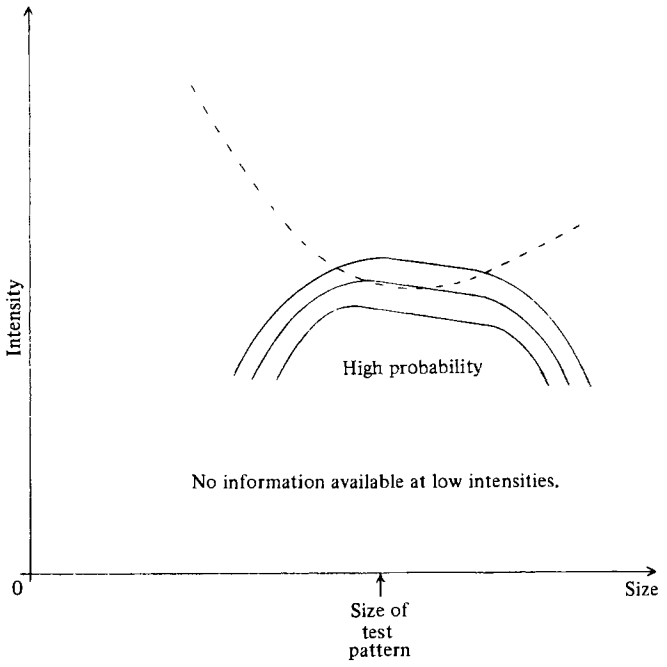


FIGURE 16. Apparent distributions of size and intensity plotted as contours of constant probability of occurrence (see text).

as the ratio of the peak velocity in the pattern to $(\overline{u^2})^{\frac{1}{2}}$ measured at the same value of $Z^*$. The diagram also shows the variation of the number of samples included in the average. For the range covered, the number of samples changes by a factor of about eight, whereas the size and intensity variations are less than 20 % of their respective mean values. This slow variation of the averaged peak velocity with the number of samples suggests a distribution of intensities which falls quite steeply to zero at the high-intensity limit. It seems, for example, that, while structures with a peak velocity of $1{\cdot}5(\overline{u^2})^{\frac{1}{2}}$ occur quite frequently, intensities of $2{\cdot}0(\overline{u^2})^{\frac{1}{2}}$ must be very improbable. Information about the shape of the distribution at lower intensities is obviously difficult to obtain.

The most probable interpretation of the available information about the distributions of eddy sizes and intensities is illustrated in figure 16, where contours of constant probability of occurrence (solid lines) are drawn in the (size, intensity)-plane. The region inside the dashed line represents samples that would be selected by the recognition programme, when provided with a test pattern of the indicated size, for inclusion in the average.

The fractional contribution to $\overline{u^2}$ from the large eddies was estimated by calculating the correlation function $R_{uu}(Z^*, (0, y^*, 0), t^*)$ that would result from a random distribution of the averaged velocity patterns over the $(x, y)$-plane, and adjusting the amplitude of this function so that it matched the measured correlation function at large $y^{*2}+t^{*2}$. The adjusted value of $R_{uu}(Z^*, \mathbf{0}, 0)$ is then the required fractional contribution to $\overline{u^2}$. The presence of a distribution of sizes leads to a degree of uncertainty in this procedure, but the contribution seems to be approximately 20 % at $Z^* = 0{\cdot}67$. While the absence of information about the structures of low intensity prevents the

detailed determination of the distribution of this energy amongst the individual structures, it is possible to obtain some indication of the occurrence probabilities, or, equivalently, the packing density, for structures of reasonably large amplitude.

These properties should have a considerable influence on the flatness factors of the convolutions found in the recognition programme. It would be expected, for example, that if the total energy contribution were made up from widely spaced structures of correspondingly large amplitude the flatness factor would be substantially greater than 3·0 (the value expected and obtained for random numbers). Thus for the simulated signal used for figures 9(*a*, *b*), having eddies with velocities of $\pm$ 1·0 r.m.s. unit and a 5 % packing density, a flatness factor of 6·9 was obtained.

The turbulence signals invariably yielded flatness factors between 2·9 and 3·1. Simulated signals were constructed with eddies giving a 20 % contribution to $\overline{u^2}$ (as found in the turbulence), and the individual intensities and corresponding packing densities adjusted to obtain flatness factors in the above range. It was found that the eddies had to be non-overlapping, and packed at a density of at least 30 %. It is not possible to construct signals of the specified type with packing densities significantly greater than this value, as it seems to be rather close to the average maximum density that can be achieved with non-overlapping random packing. Higher densities require some degree of organization and, in the present context, would imply preferred positions for nearest neighbours. An additional test, performed at a density of 100 % using non-overlapping box eddies, arranged as randomly as 100 % packing allows, also yielded a flatness factor in the required range.

The evidence from the statistical properties of the recognition programme indicates, therefore, that the structures must be packed at a density where the nearest-neighbour spacing is unlikely to be greater than the size of the individual structures. It may well be the case that, in addition to the pairing discussed in § 6, more complex local groupings tend to occur.

## 8. Further developments

In the present series of experiments, the ensemble-averaging technique has been applied only to the streamwise velocity component. A simple modification would enable the ensemble-averaged patterns of all three velocity components to be extracted from data obtained using an array of X-wires. One suspects, however, that few would relish the prospect of performing such experiments.

Another possibility is the use of the pattern-recognition technique on data obtained by conditional sampling, to investigate the relationship between the large eddies and flow features detectable from 'instantaneous' conditions (e.g. the interface between turbulent and irrotational fluid). One problem that should be soluble by this method is the question of whether the regions of the flow into which the energy at high wavenumbers is concentrated tend to occur in preferred positions relative to the large eddies.

The author would like to thank Mr W. G. Garner for the preparation of the hot-wire probes, and the construction of the mechanical apparatus. The author is greatly indebted to Dr A. A. Townsend for much invaluable advice. The work was supported by the Science Research Council.

## REFERENCES


BLACKWELDER, R. F. 1979 Dynamic measurements in unsteady flows. In *Proc. Dynamic Flow Conf.* 1978, *Marseilles and Baltimore*, p. 173.

BRUUN, H. H. 1971 *J. Sci. Instrum.* **4**, 815.

CHAMPAGNE, F. H., SLEICHER, C. A. & WEHRMANN, O. H. 1967 *J. Fluid Mech.* **28**, 153.

DAVIES, P. O. A. L. & YULE, A. J. 1975 *J. Fluid Mech.* **69**, 513.

FAVRE, A. J., GAVIGLIO, J. J. & DUMAS, R. J. 1957 *J. Fluid Mech.* **2**, 313.

FAVRE, A. J., GAVIGLIO, J. J. & DUMAS, R. J. 1958 *J. Fluid Mech.* **3**, 344.

FISHER, M. J. & DAVIES, P. O. A. L. 1964 *J. Fluid Mech.* **18**, 97.

GRANT, H. L. 1958 *J. Fluid Mech.* **4**, 149.

KOVASZNAY, L. S. G., KIBENS, V. & BLACKWELDER, R. F. 1970 *J. Fluid Mech.* **41**, 283.

LUMLEY, J. L. 1965 Atmospheric turbulence and radio wave propagation. In *Proc. Int. Colloq. Moscow*, p. 166.

MUMFORD, J. C. 1973 Some properties of the plane turbulent jet. Ph.D. dissertation, University of Cambridge.

PAYNE, F. R. & LUMLEY, J. L. 1967 *Phys. Fluids Suppl.* **10**, S194.

SABOT, J. & COMTE-BELLOT, G. 1976 *J. Fluid Mech.* **74**, 767.

STERNBERG, J. 1967 *Phys. Fluids Suppl.* **10**, S146.

TOWNSEND, A. A. 1970 *J. Fluid Mech.* **41**, 13.

TOWNSEND, A. A. 1976 *The Structure of Turbulent Shear Flow*. Cambridge University Press.

TOWNSEND, A. A. 1979 *J. Fluid Mech.* **95**, 515.

TRITTON, D. J. 1967 *J. Fluid Mech.* **28**, 439.

WALLACE, J. M., BRODKEY, R. S. & ECKELMANN, H. 1977 *J. Fluid Mech.* **83**, 673.

WYGNANSKI, I. & FIEDLER, H. E. 1969 *J. Fluid Mech.* **38**, 577.